Statistical analysis of the magnetization processes in arrays of electrodeposited ferromagnetic nanowires

Y. Henry* and A. Iovan

Institut de Physique et Chimie des Matériaux de Strasbourg, CNRS and Université Louis Pasteur, 23, rue du Loess, F-67037 Strasbourg Cedex, France

J.-M. George

Unité Mixte de Physique CNRS-THALES, domaine de Corbeville, F-91404 Orsay, France

L. Piraux

Département des Sciences des Matériaux et des Procédés, Université Catholique de Louvain, Place Croix du Sud 1, Louvain la Neuve B-1348, Belgium

We present a statistical analysis of the magnetization processes in arrays of 22-μm-long, 40-nm-wide Co and Ni nanowires, with parallel-to-wire magnetic anisotropy, electrodeposited into porous polycarbonate membranes. This analysis is based on usual magnetization measurements taken with a magnetic field applied parallel to the average wire direction. It is shown that the magnetization curves may contain, in proportions which depend on the magnetic history of the arrays prior to the measurement, two contributions corresponding, respectively, to single-domain wires reversing their magnetization and to wires initially in a multidomain state which are remagnetized to saturation. Despite the extremely large number of wires involved, these two contributions exhibit clearly discernible substructures. These are related to the different and rather weakly distributed characteristic fields that describe the reversal and remagnetization processes: the nucleation and propagation fields. Numerical simulations of the magnetization curves are carried out which allow one to deduce the statistical distributions of these fields. From this modeling of the experimental data, it is shown that two distinct kinds of defects with very different pinning strength are certainly present in the nanowires. Finally, the analysis of the magnetization curves also provides accurate information concerning the distribution of wire orientation in the polycarbonate templates.

I. INTRODUCTION

Nanomagnets are currently receiving considerable attention. This is first due to their undeniable technological interest: They will soon find applications in high density magnetic recording media, miniaturized sensors, and spintronic devices. The second reason, more fundamental, is that nanomagnets often show unusual properties, compared to bulk or thin film magnetic materials, the understanding of which is of primary importance from theoretical and practical viewpoints.

Advanced lithographic techniques are usually employed to make periodic arrays of submicronic magnetic dots, wires, and pillars.[1,2] However, these are relatively expensive, time consuming, and cumbersome. An alternative approach for producing nanoscaled materials is electrodeposition into templates with nanometer-wide cylindrical pores, such as anodic alumites[3] and track-etched polymer membranes.[4–7] This is a low-cost and high yield technique, particularly suitable for large-area production of nanostructures with very large aspect ratio, i.e., nanowires.

Ferromagnetic nanowires fabricated in this way have already been investigated extensively over the last decade.[3,7] Some of the fundamental issues tackled were how the magnetization configuration of an extremely long cylindrical magnet is affected when its diameter becomes comparable to key magnetic length scales, such as the domain wall width, and how magnetocrystalline anisotropy influences the internal domain structure in such elongated objects (see, for example, Ref. 8).

Experimental evidence[9–13] was also given that the magnetization reversal in these nanowires does not occur through coherent rotation or curling, that is, delocalized reversal modes extending throughout the entire wire, which are exact solutions of the nucleation problem in ideal homogeneous ellipsoids of revolution.[14,15] This rather occurs through the creation of a localized reversed nucleus, followed by a propagation, involving pinning or not.[10,13] The reason for this localization effect might be that real wires exhibit strong deviations from the ideal shape and structure. These deviations result from various types of disorder, such as diameter fluctuations, crystalline defects, or irregular geometrical features at the wire ends. Although magnetization processes localized in the vicinity of imperfections are not favorable from the point of view of exchange energy, since they involve very inhomogeneous magnetization states, it was argued that they may become more favorable, as compared to delocalized processes, due to locally reduced anisotropy and/or magnetostatic energies.[3,16] However, recent micromagnetic simulations also predicted that the magnetization reversal occurs by means of nucleation at the ends and subsequent soliton-*like* propagation of 180° domain walls, even in defect free nanowires.[17]

Most of the valuable information available on the magne-

tization processes in electrodeposited nanowires was obtained from the direct study of individual objects using rather sophisticated experimental techniques: MicroSQUID's, (superconducting quantum interference devices),[9,10] magnetic force microscopy,[11,13] and magnetoresistance measurements.[12,13,18] In this paper, we show how a cautious analysis of straightforward magnetization measurements taken on large arrays of such nanowires can, yet in favorable circumstances (that will be clarified in the course of the paper), yield precious statistical information, complementary to those gained from the aforementioned techniques.

The samples studied in this work consist of arrays of millions of 40-nm-thick Ni and Co nanowires with parallel-to-wire easy axis of magnetization. Though the single-domain state is the most commonly one associated with these wires, a multidomain structure can be induced after saturation in a perpendicular-to-wire magnetic field.[8] The (re)magnetization curves taken on these nanowire arrays may thus contain, in proportions which depend on their magnetic history, contributions from single-domain wires reversing their magnetization and from multidomain wires being remagnetized. It is shown here that, despite the extremely large number of wires involved, the (re)magnetization curves exhibit several clearly discernible substructures. These are related to the rather weakly distributed characteristic fields describing the reversal and remagnetization processes.

The paper is divided as follows. Relevant details on the fabrication and structural properties of the nanowires are given in Sec. II. In Sec. III, we first recall what is known about the magnetic anisotropy and the possible domain structures in the Ni and Co wires studied and we then demonstrate the irreversible character of the magnetization processes discussed in the following sections. In Sec. IV, we describe our experimental procedure and present a quantitative analysis of the magnetization curves measured, from which an estimate of the dispersion in the wire orientation is deduced. In Sec. V, numerical simulations of the magnetization curves are presented, which allow one to explain in detail the origin of the substructures observed in these curves. Finally, we give our conclusions in Sec. VI.

II. FABRICATION, MICROSTRUCTURE, AND MORPHOLOGY OF THE NANOWIRES

Random arrays of ferromagnetic nanowires were synthesized by electrodeposition of Co or Ni into the pores of homemade track-etched polycarbonate membranes. In comparison with most polycarbonate porous templates available commercially, the membranes used show narrower size distribution and improved shape regularity and parallel alignment of the pores. A detailed description of the template fabrication, which involves irradiation with heavy ions and chemical etching of amorphous polycarbonate films, may be found in Ref. 19; only relevant information will thus be given thereafter. A particularly important feature is that the irradiation was performed under parallel ion beam at normal incidence with respect to the plane of the polycarbonate films so that the dispersion in the direction of the ion tracks, hence in the direction of the pores, is very small (an estimate of this
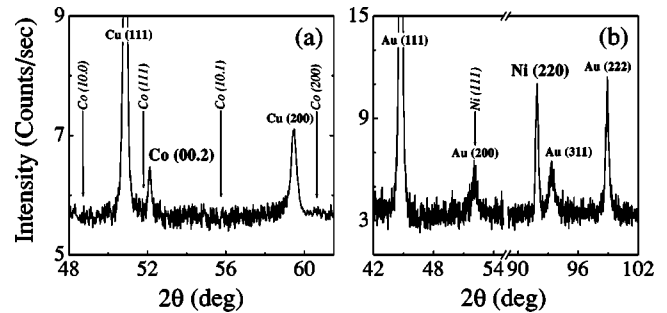

FIG. 1. $\theta/2\theta$ XRD spectra recorded on arrays of (a) Co and (b) Ni nanowires with the diffraction vector perpendicular to the plane of the membrane, i.e., parallel to the average wire direction ($\lambda = 0.178897$ nm). Cobalt and nickel possess their normal equilibrium phases, hcp and fcc, respectively, with strongly dominating textures, [0001] and [110], respectively. From the position of the diffraction peaks ($2\theta = 52.13°$ for Co and $2\theta = 91.90°$ for Ni), one deduces lattice parameters of $c_{Co} = 0.4072$ nm and $a_{Ni} = 0.3520$ nm respectively, very close to the bulk values of 0.4069 nm and 0.3517 nm. Note also the presence of diffraction peaks associated with the (a) Cu and (b) Au films which served as cathodes during electrodeposition.

dispersion may be obtained from the analysis of magnetic measurements; see Sec. IV D). The etching conditions were optimized to produce cylindrical pores with average diameters of 40 nm.

For the nanowire growth, a thin noble metal film was deposited by thermal evaporation on one side of the porous membranes to serve as a cathode. The filling of the pores was then performed by electrodeposition of Co or Ni under potentiostatic control using a conventional three-electrodes cell.[5] More details on the growth conditions are given in Refs. 8 and 20. For the present study, we used 22-μm-thick polycarbonate membranes with a porosity of 0.5% and an areal density of 10^8 pores per square centimeter. The average spacing between the pores is then of the order of 1 μm. The surface area of porous membrane exposed to the electrolyte during the growth was in the range of 0.1–0.3 cm^2 so that the arrays of nanowires consist of 10–30 million elements.

A structural characterization of the Co and Ni nanowire arrays was performed using x-ray diffraction (XRD) and transmission electron microscopy (TEM). Cobalt nanowires with diameters in the range of 30 to 40 nm were shown to be made of large crystal grains, several micrometers long, extending across the full wire cross section.[8] These Co grains have the bulk stable hcp structure and are preferentially oriented so that their crystallographic c axis is parallel to the wire ([0001] texture; see Fig. 1(a)). In comparison with Co nanowires, Ni nanowires are made of smaller crystal grains. These possess their normal equilibrium phase, that is fcc. In the case of Ni, XRD spectra reveal the existence of a strong [110] texture [Fig. 1(b)].

Besides the microstructure, an important parameter that influences the magnetization processes in nanostructures is the morphology. The nanowires studied have relatively regular cylindrical shape [Fig. 2(a)]. Yet they exhibit shape irregularities. First, both Ni and Co nanowires show roughness at their surface. In particular, they contain constrictions, that
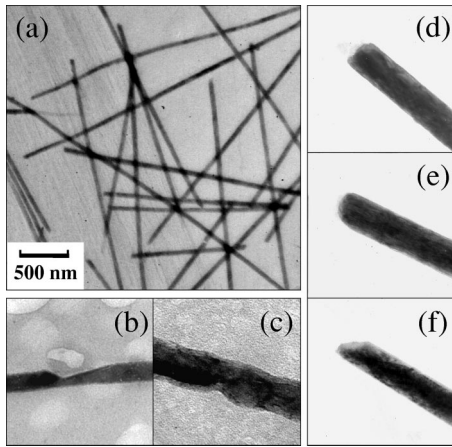
FIG. 2. Bright field TEM images of Co nanowires freed from the polycarbonate template. (a) Large scale view. (b) and (c) Close views of constrictions. (d)–(f) Close views of extremities with different typical shapes: (d) flat, (e) round, and (f) pointed.

is, local reductions of their diameter [Fig. 2(b,c)]. Second, there exists a spread (from wire to wire) in their mean diameter (averaged along the wire length) which is of the order of 10–20 %, as estimated from scanning electron microscopy images. Finally, the nanowires show irregular features at their extremities [Fig. 2(d–f)].

III. MAGNETIC ANISOTROPY, DOMAIN STRUCTURES, AND MAGNETIZATION PROCESSES

As a necessary preliminary to the analysis of the magnetization measurements taken on the Ni and Co nanowire arrays, which is the topic of the next sections, hereafter we recall some previous results concerning the basic magnetic properties of these nanowires, namely their magnetic anisotropy and possible domain structures.

A. Magnetic anisotropy

The cylindrical nanowires studied have a length to diameter ratio of $L/\phi \simeq 550$ ($L=22$ μm, $\phi=40$ nm nominally). Their very elongated shape is at the origin of a large shape anisotropy, closely approaching that of infinitely long cylinders πM_S^2, which favors an alignment of the magnetization along the wire axis (uniaxial anisotropy). Due to the intrinsically low crystal anisotropy of fcc Ni and the absence of significant magnetoelastic effect, shape (demagnetizing energy) is the only important source of magnetic anisotropy in Ni nanowires ($\pi M_S^2 = 7.4 \times 10^5$ erg/cm^3 with $M_S = 485$ emu/cm^3), at room temperature.[20]

In Co nanowires, crystal anisotropy is of the same order of magnitude as shape anisotropy ($\pi M_S^2 = 6.2 \times 10^6$ erg/cm^3 with $M_S = 1400$ emu/cm^3). It is of uniaxial symmetry and amounts to $K \simeq 2 \times 10^6$ erg/cm^3 at room temperature, as deduced from magnetic torque measurements.[8] Thus crystal anisotropy certainly plays a role in Co nanowires. However, the crystal easy axis of magnetization (c axis) being parallel to the wire ([0001] texture of Co), this role may be considered
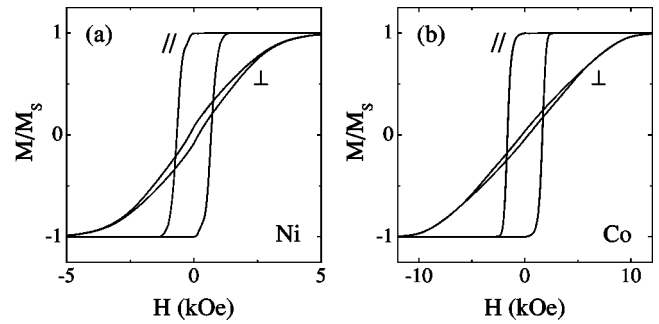

FIG. 3. Room temperature hysteresis loops measured on arrays of (a) Ni and (b) Co nanowires with the magnetic field applied parallel ($\parallel$) and perpendicular ($\perp$) to the average wire direction (normal to the membrane). The nanowires have a nominal diameter of 40 nm.

as limited: Crystal anisotropy helps in maintaining the magnetization aligned along the wire axis and simply reinforces shape anisotropy.

B. Domain structures

Because the overall anisotropy is in both cases in favor of a longitudinal orientation of the magnetization, Ni and Co nanowires behave very similarly. In particular, the domain structures they form are qualitatively identical. After saturation in a parallel-to-wire magnetic field [longitudinal remanent state, $\theta_H = 0°$ (180°)], Ni and Co nanowires are in a single-domain state with longitudinal magnetization. This is first evidenced by the parallel-to-wire hysteresis loop squareness M_r/M_S (the remanent magnetization to saturation magnetization ratio) very close to unity measured on assemblies of such wires (Fig. 3). This is further confirmed by magnetic force microscopy (MFM) images taken on single nanowires after the dissolution of the polycarbonate template, an example of which is shown in Fig. 4(a). These images consist only of complementary dark and bright monopolar contrasts spanning the wire extremities, which indeed correspond to the pole distributions of opposite polarities located on the end faces of an axially magnetized cylindrical bar magnet.[8]

When being brought to the transverse remanent state by applying momentarily a saturating magnetic field perpendicular to the wire axis ($\theta_H = 90°$), Ni and Co nanowires no longer stay in a single-domain state. They rather split into several axially magnetized domains with alternating magnetization direction.[8] These domains, which are forced to meet head-on because of the lateral confinement of the magnetization, are separated by 180° walls that carry a large amount of magnetic charges (their probable micromagnetic structure is shown in Fig. 2 of Ref. 17). These are revealed by intermediate monopolar MFM contrasts of alternating polarity, much more intense than the end contrasts [Fig. 4(d)]. Notice that the strongly reduced total magnetic moment associated with the multidomain structure of Fig. 4(d) is consistent with the very low transverse remanent magnetization measured on arrays of wires located in their polycarbonate templates (Fig. 3).

The formation of such multidomain structures may be explained as follows. As the strength of the applied field is
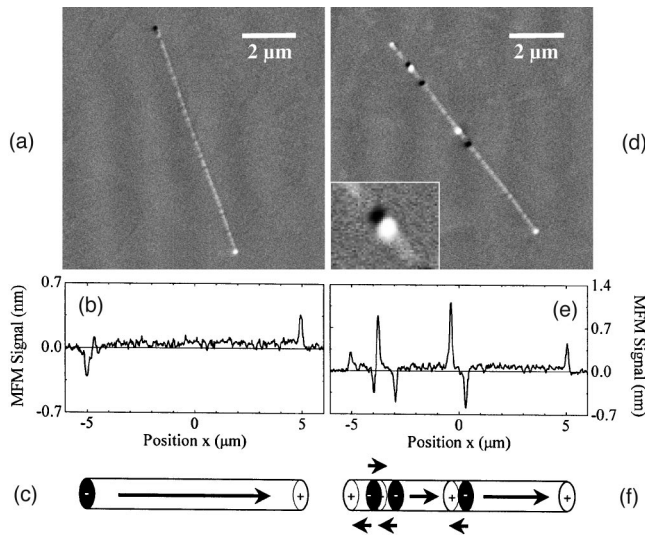
FIG. 4. [(a) and (d)] MFM images, [(b) and (e)] densitometer traces along the wire axis and [(c) and (f)] schematic magnetization distributions for a 10-μm-long, 40-nm-wide Co wire fragment after the application and removal of (a)–(c) an axial saturating field (longitudinal remanent state), and (d)–(f) a transverse saturating field of 1.4 T (transverse remanent state). The MFM images were recorded with a Nanoscope III^{TM} scanning probe microscope equipped with a magnetically hard CoCr-coated tip magnetized along its axis, and applying the tapping/lift^{TM} interlace technique developed by Digital Instruments. The weak bright contrast visible all along the wire in (a) and (d) is due to residual topographical interactions (Ref. 8). The inset in (d) is a close view of the adjacent black and white contrasts located 1 μm below the upper end of the wire fragment.

reduced, starting from the transverse saturation, the magnetization, which is subjected to a strong torque due to the parallel-to-wire magnetic anisotropy, rotates progressively toward the wire axis. If the external field is perfectly oriented perpendicular to the wire (or at a very small angle from the plane normal to the wire) so that the two axial directions colinear to the wire are equivalent, any two regions of the wire which are sufficiently decoupled from each other to behave independently may have their magnetization vectors rotate in opposite directions (clockwise and counterclockwise). If this is the case, these two regions eventually give rise in zero field to two domains of opposite axial magnetization, necessarily separated by a 180° wall. Such a splitting in domains of opposite axial magnetization is all the more likely to occur as the length of the nanowires ($L = 22$ μm) is very much larger than the exchange length ($\Lambda \simeq 3$ nm for Co and $\Lambda \simeq 8$ nm for Ni).

Importantly, it is known from MFM experiments that there exists only a very narrow range of field angle [$(90 - \epsilon) \leqslant \theta_H \leqslant (90 + \epsilon)$ with $0 \leqslant \epsilon \ll 90°$] for which multidomain structures form in the way just described. As soon as the angle δ_H between the field and the plane normal to the wire gets large ($|\delta_H| > \epsilon$) that of the two directions colinear to the wire axis which is parallel to the longitudinal component of the field is naturally favored. Upon reduction of the field strength the magnetization then rotates as a whole toward this favored direction and the resulting remanent state

is without fail single-domain. Finally, it is noteworthy that multidomain structures similar to those described above form also after demagnetization with an alternating field of slowly decreasing amplitude applied along the normal to the wire axis (transverse demagnetization).

C. Magnetization processes

1. Results from previous works

As a last prerequisite to the understanding of the magnetization measurements presented in the following sections, we also summarize next previous results on the magnetization processes that may occur in the nanowires *when submitted to a longitudinal external field*.[13,18] Due to the one-dimensional-like geometry of the wires these processes are rather simple. First, it was demonstrated that the domain walls shown in Fig. 4(d), i.e., domain walls induced after transverse saturation, are initially located at pinning sites of varying strength. A particular domain wall may be moved along the wire by applying a magnetic field larger than the depinning or propagation field (or wall-motion coercive field) of the site where it is located. A propagating wall stops only if it encounters a pinning center the strength of which is larger than the applied field.

The remagnetization to saturation of a wire split into several domains happens in the following way. The two walls that delimit inner domains with magnetization antiparallel to the external field move toward each other until they meet and the antiparallel domain is annihilated. Antiparallel end domains, which are delineated by a wire extremity on one side and a domain wall on the other side, may be annihilated in two ways: (i) the existing domain wall may move toward the wire extremity, where it is eventually expelled; or (ii) a second domain wall may be nucleated at the wire extremity, in which case the annihilation occurs when this nucleated wall meets the one existing initially.

During the magnetization reversal of a single-domain nanowire a similar pinning-propagation process occurs with domain walls forced through a one-dimensional dispersion of defects, a maximum of two walls (one per extremity) being nucleated from the wire extremities. In the absence of definite information regarding their intimate micromagnetic structure, we will assume in what follows that the domain walls formed after the application of the transverse saturating field and those nucleated while applying a longitudinal field are similar, at least as far as their pinning on defects is concerned. Micromagnetic simulations[17] support this assumption.

2. Reversible versus irreversible processes

The magnetization processes just described were inferred from MFM observations and magneto-transport measurements carried out on single nanowires.[13,18] They are purely irreversible. To corroborate them and demonstrate that the magnetization processes at stake in our nanowires when these are submitted to longitudinal fields are effectively fully irreversible, demagnetizing and magnetizing remanence curves were measured on large arrays of such objects. While
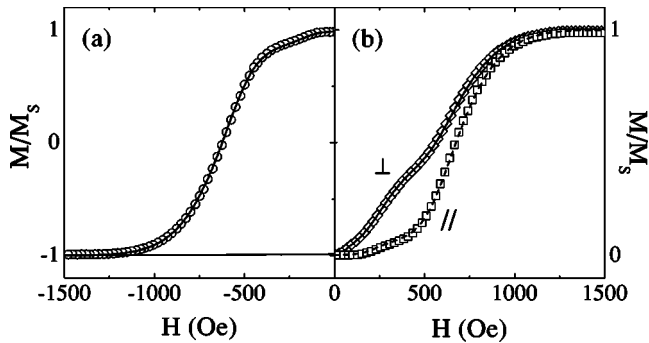
FIG. 5. Magnetization measurements taken on an array of Ni nanowires. The external field is applied along the normal to the plane of the membrane, i.e., along the average direction of the wire axes. (a) Major hysteresis loop (solid line) and demagnetization remanence curve (circles). (b) First magnetization curves (lines) and magnetizing remanence curves (symbols) after demagnetization with an ac field applied parallel (dashed line, squares) and perpendicular (solid line, diamonds) to the average wire direction.

a hysteresis loop is generally a consequence of both reversible and irreversible processes, remanence is a natural consequence of irreversible processes only. Remanence curves are thus useful tools by which to separate the two kinds of processes.[21] The dc demagnetizing remanence $M_d(H)$ is obtained by the successive application and removal of a reverse direct field $-H$ to the remanent state after positive saturation, while the magnetizing (isothermal) remanence $M_m(H)$ is obtained by applying and then removing a positive field H to an unmagnetized state. Both $M_d(H)$ and $M_m(H)$ give a measure of the amount of magnetization that has switched irreversibly in a given field H. The unmagnetized state considered here is an ac demagnetized state created by applying an alternating field of slowly decreasing amplitude either perpendicular to the average wire direction (normal to the plane of the membrane), in which case both single-domain and multidomain nanowires occur in the array (see Secs. III B and IV B), or parallel to the average wire direction, in which case the nanowire assembly essentially divides into two equally large populations of single-domain objects with opposite magnetizations.[22] Figure 5 illustrates the fact that for our nanowire arrays the demagnetizing and magnetizing remanence curves coincide well with the major hysteresis loop $M(H)$ and first magnetization curve $M_{ini}(H)$ respectively. This proves that $M(H)$ and $M_{ini}(H)$ do indeed not contain large reversible magnetization components.

Still a very small deviation between the magnetization curves and the corresponding remanence curves may be detected (Fig. 5), especially at fields larger than 1 kOe $[|M_d(H)|<|M(H)|, M_m(H)<M_{ini}(H)]$. This reveals the existence of a yet detectable reversible magnetization component in $M(H)$ and $M_{ini}(H)$. Nevertheless, this deviation does not jeopardize our interpretation of the magnetization processes in longitudinal fields as it may be safely ascribed to the fact that not all of the nanowires in the array have their axis perfectly aligned along the normal to the plane of the membrane, which is the direction of the applied field in Fig. 5. When reducing the field to zero for remanence measurement, the magnetization in those wires the revolution axis of
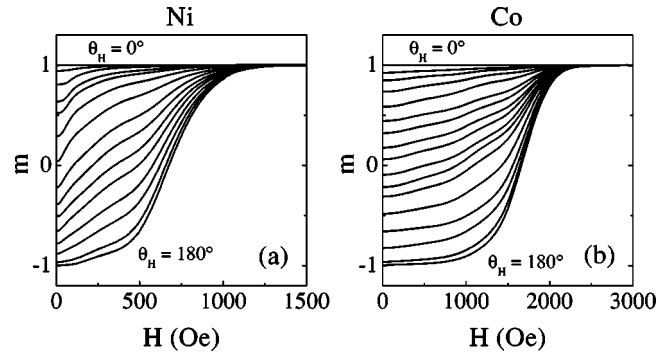

FIG. 6. First magnetization curves measured on (a) a Ni nanowire array and (b) a Co nanowire array with the external field **H** applied along the normal to the plane of the membrane, after saturation in a field of varying orientation (see the text for details).

which is not perfectly parallel to the normal to the membrane rotates slightly away from the field direction (toward the revolution axis), so as to minimize anisotropy energy, hence giving rise to a tiny reduction of magnetic signal. Given its very small size, we will neglect this reversible magnetization component in the analysis that follows.

IV. MAGNETIZATION MEASUREMENTS: RESULTS AND ANALYSIS

A. Experimental procedure

The magnetization measurements analyzed in this section were carried out at room temperature using a MicroMag^{TM} Model 2900 alternating gradient force magnetometer from Princeton Measurement Corporation. To make easier the description of the geometry of these measurements, let us assume that the polycarbonate membranes were lying in the horizontal xy plane. In these conditions, the average direction of the wire axes was parallel to the vertical $\hat{\mathbf{z}}$ axis. All of the measurements were taken with the external field **H** parallel to the upwardly directed normal to the membrane $\hat{\mathbf{n}}_\uparrow$ $[\mathbf{H}=(0,0,H)$ with $H \geq 0]$. Prior to the measurement, the wire arrays were submitted to a saturating field $\mathbf{H}_{sat}$ of 1.4 T applied at an angle θ_H from $\hat{\mathbf{n}}_\uparrow$ $(0 \leq \theta_H \leq 180°)$. Starting systematically from zero, the field strength was progressively increased (with a moderate sweep rate of 20 Oe/s for the Ni nanowires and 50 Oe/s for the Co nanowires) until the saturation of the magnetization was reached. For convenience all the magnetization values and curves discussed in the rest of this paper will be normalized to the saturation magnetization value M_S $(m=M/M_S)$.

B. History dependence of the longitudinal magnetization curve

Figure 6 shows sets of first magnetization curves obtained following the experimental procedure described above for characteristic Ni [Fig. 6(a)] and Co [Fig. 6(b)] nanowire arrays. If one examines closely these curves, one may see that they are made of several contributions the amplitudes of which change when the angle θ_H of the saturating field $\mathbf{H}_{sat}$ is varied. This becomes obvious if instead of looking at the

FIG. 7. Ni nanowire array. (Open circles) Derivative with respect to H of some of the first magnetization curves $m(H)$ shown in Fig. 6(a). (Solid lines) Fits and decompositions of these $\chi(H) = dm(H)/dH$ curves in terms of SDR and MDR components (see the text for details). Note that the lowest curve was magnified by a factor of 2.
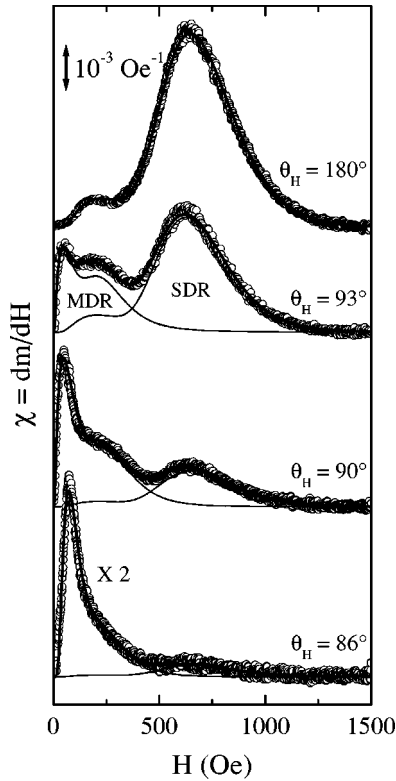

FIG. 8. Co nanowire array. (Open circles) Derivative with respect to H of some of the first magnetization curves $m(H)$ shown in Fig. 6(b). (Solid lines) Fits and decompositions of these $\chi(H) = dm(H)/dH$ curves in terms of SDR and MDR components (see the text for details). Note that the two bottommost curves were magnified by a factor of 2 and a factor of 10, respectively.

$m(H)$ curves one rather looks at the (reduced) susceptibility curves defined as $\chi(H) = dm(H)/dH$ (Figs. 7 and 8).

Before proceeding with the analysis of these $\chi(H)$ curves, on which we will focus henceforth, a few words should be said about their physical meaning. We demonstrated in Sec. III C that, in good approximation, the magnetization curves measured on nanowires with an external field applied along the normal to the membrane contain only an irreversible component $[m(H) = m_d(H) = m_{irr}(H)]$. Therefore, $\chi(H) = dm(H)/dH$ is equivalent to the (reduced) irreversible susceptibility $\chi_{irr}(H) = dm_{irr}(H)/dH$ which, in the case of assemblies of magnetic particles, is directly related to the switching field distribution.[23] In the sequel, the $\chi(H)$ curves will thus be regarded implicitly as such.

Let us now come back to the different contributions that these $\chi(H)$ curves contain. We shall first define them and elucidate their origin. For $\theta_H = 180°$, the first magnetization curve is equivalent to the increasing field branch of the major hysteresis loop. Thus we know for certain that all of the nanowires are initially in a single-domain state (see Sec. III B) with the magnetization (almost) antiparallel to the applied field **H**. Therefore, the first contribution that we may identify is the one that shows up at high fields (the only one present for $\theta_H = 180°$). It can undoubtedly be attributed to the reversal of single-domain wires. In the sequel this contribution will be referred to as the single-domain-reversal
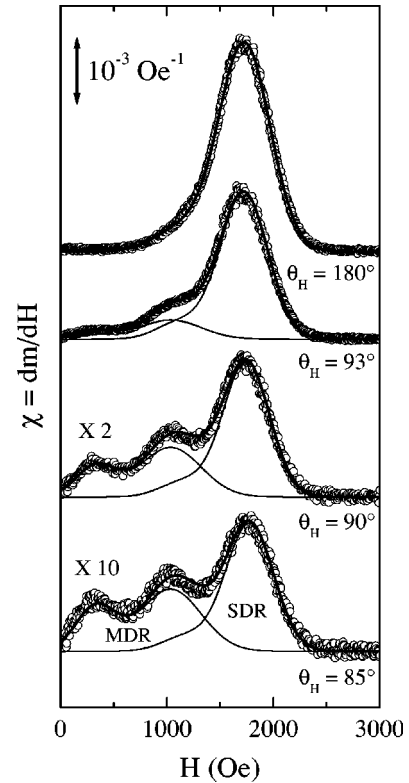
(SDR) component and labeled $\chi_{SDR}(H)$ ($= dm_{SDR}(H)/dH$). In the case of the Ni nanowire array (Fig. 7), it has a clear double-peak shape. We will demonstrate in Sec. V that this results from the conjunction of two properties. First, the magnetization reversal occurs schematically in two consecutive steps (see Sec. III C): The nucleation and pinning of domain walls followed by the propagation and expulsion (or annihilation) of these walls. Second, the statistical distributions of nucleation fields $P_n(H_n)$ and propagation fields $P_p(H_p)$ associated with the Ni nanowire array only weakly overlap. In contrast, the overlapping of the distributions $P_n(H_n)$ and $P_p(H_p)$ is larger for the Co nanowire array. Hence the SDR component exhibits only one peak, but with a pronounced shoulder on the low field side (Fig. 8), reminiscent of the fact that the typical (most probable) value of H_n is smaller than that of H_p [at this stage, it is assumed that $P_n(H_n)$ and $P_p(H_p)$ are unimodal and symmetrical distributions].

In addition to the SDR component, a second contribution shows up at smaller fields as θ_H is diminished. This additional contribution has also a well-defined double-peak shape.[24] Moreover, as illustrated in Figs. 7 and 8, this becomes more and more important as θ_H approaches $90°$. Then it can be safely ascribed to the remagnetization of nanowires initially in a multidomain state, as a the result of the application of a transverse saturating field prior to the measurement (see Sec. III B). In the sequel, we will term this com-

ponent multidomain-remagnetization (MDR) and label it $\chi_{MDR}(H)$ $[=dm_{MDR}(H)/dH]$. To account for the fact that the remagnetization of multidomain nanowires usually occurs in fields smaller than the reversal of single-domain wires, one may simply notice that the remagnetization does not require the nucleation of domain walls from the wire extremities, since walls already exist, whereas the reversal does. However, only numerical simulations as those reported in section V will give a comprehensive explanation of this phenomenon as well as of the double-peak structure of the MDR component.

As may be seen in Figs. 7 and 8 the SDR component does not vanish entirely for $\theta_H = 90°$. This is essentially due to the imperfect parallel alignment of the nanowires. Indeed, if all of the wires in an array were parallel, they would all (or almost all) split into domains following the application of the saturating field at $\theta_H = 90°$. Hence the vast majority of them would contribute to the MDR component, a fact disproved experimentally.

More generally, due to the dispersion in the wire orientation, which is very small as we will show, the arrays are constituted of three categories of nanowires after the application of $\mathbf{H}_{sat}$. (i) Those nanowires for which the angle between their axis and $\mathbf{H}_{sat}$ is in the range $[90-\epsilon, 90+\epsilon]$ (with $0 \leq \epsilon \ll 90°$) are in a multidomain (MD) state. Then, they will contribute to the MDR component of the first magnetization and susceptibility curves. (ii) Those nanowires for which the angle between their axis and $\mathbf{H}_{sat}$ is larger than $90+\epsilon$ are in a single-domain state. That of the two directions colinear to their axis which is naturally favored when removing $\mathbf{H}_{sat}$ being the one pointing downward, their magnetization is (almost) antiparallel to $\mathbf{H}$ (SD$_\downarrow$ state). Therefore they will contribute to the SDR component of the first magnetization and susceptibility curves. (iii) Finally, those nanowires for which the angle between their axis and $\mathbf{H}_{sat}$ is smaller than $90-\epsilon$ are in a single-domain state too. However, since that of the directions colinear to their axis which is favored when turning off $\mathbf{H}_{sat}$ is the one pointing upward, their magnetization is (almost) parallel to $\mathbf{H}$ (SD$_\uparrow$ state). As a consequence, they will not give rise to any change of magnetization upon increasing H, hence will not manifest themselves in the $\chi(H)$ curve. They will only contribute to the longitudinal remanent magnetization $m_0 = m(H=0)$ measured immediately after the application of $\mathbf{H}_{sat}$.

C. Decomposition of the longitudinal magnetization curve

From the previous discussion it is clear that the remanent magnetization m_0, the integral of the SDR component $\chi_{SDR}(H)$ over H (from 0 to infinity), Δm_{SDR}, and that of the MDR component $\chi_{MDR}(H)$, Δm_{MDR}, are intimately related to the initial fractions of nanowires in the SD$_\uparrow$, SD$_\downarrow$, and MD magnetic states. As will be show next (Sec. IV D) the variation of these quantities as a function of θ_H may yield important information on the dispersion of the wire directions and values for the critical angle ϵ. However, obtaining the amounts of nanowires in the SD$_\downarrow$ and MD states first requires one to separate the SDR and MDR components. In practice, this was achieved by fitting the $\chi(H)$ curves with a
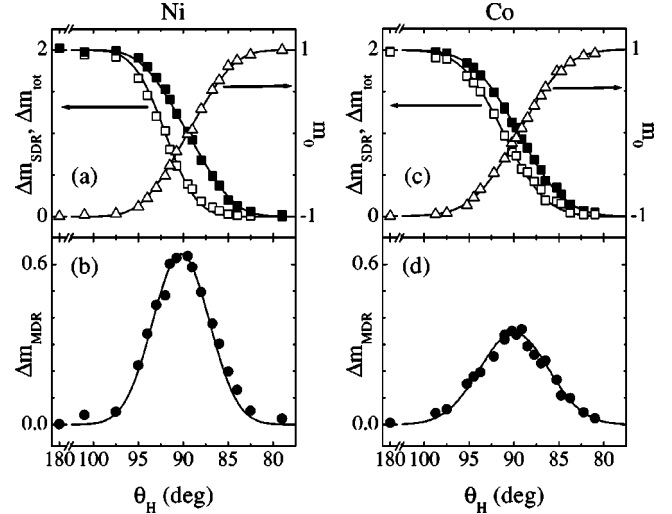

FIG. 9. Variations of [(a) and (c)] Δm_{SDR} (open squares), Δm_{tot} (solid squares), m_0 (triangles) and [(b) and (d)] Δm_{MDR} with the angle θ_H for the arrays of [(a) and (b)] Co and [(c) and (d)] Ni nanowires. The solid lines are the best possible simulations of these angular variations that could be obtained using the model described in Sec. IV D. The parameters used are $\sigma_\theta = (3.1 \pm 0.1)°$ and $\epsilon = (2.6 \pm 0.1)°$ for Ni, $\sigma_\theta = (3.5 \pm 0.1)°$ and $\epsilon = (1.6 \pm 0.1)°$ for Co.

set of four lines. Two of them were introduced to reproduce the SDR component the shape of which was assumed to be independent of θ_H and the amplitude of which only was allowed to vary (fixed positions and linewidth, and fixed ratio of the amplitudes of the two lines). The second pair of lines was used to reproduce the MDR component. For the Ni nanowire array the lines used for the fit were log-normal lines, whereas these were Gaussian lines for the Co nanowire array. As shown in Figs. 7 and 8, successful fits of the $\chi(H)$ curves could be obtained in this way. Since the SDR and MDR components do not overlap strongly, one may be quite confident in the accuracy of the decomposition.

In the case of the Co nanowire array (Fig. 8), the shape of the MDR component as deduced from the fitting procedure was found almost independent of θ_H: The position and width of two lines necessary to reproduce it could be left unchanged in the fit, only their relative amplitudes had to be slightly adjusted when varying θ_H. It is clear from Fig. 7 that no such invariance of the shape of the MDR component occurs for the Ni nanowire array. In particular, it is obvious that the relative amplitudes of the two peaks the MDR component is made of change drastically with θ_H. A tentative explanation of this phenomenon will be given in Sec. V, after the origin of the double-peak shape of the MDR component be elucidated.

D. Modeling of the history dependence of the magnetization curve components

The variation of m_0, Δm_{SDR}, Δm_{MDR} and $\Delta m_{tot} = \Delta m_{SDR} + \Delta m_{MDR}$ as a function of θ_H is presented in Fig. 9. A simple model was developed to simulate this angular variation. In this model, only the initial magnetic state and the final magnetic state of the nanowires are of importance. The details of the magnetization processes which lead from

the former to the latter are deliberately ignored: The model aims at reproducing only the sizes of the SDR and MDR components of the $\chi(H)$ curves, i.e., Δm_{SDR} and Δm_{MDR}, not their shapes. The model obeys the rules described previously which determine in what magnetic state a nanowire finds itself after the application of the saturating field $\mathbf{H}_{sat}$ (see Sec. IV B). Moreover, it is based upon the following additional assumptions. The arrays contain N nanowires and have a (reduced) saturation magnetization of N units (one unit is equal to $1/N$). A nanowire in a multidomain state has zero net magnetic moment,[25] hence does not contribute to the remanent magnetization m_0. Its remagnetization gives rive to an increase of total magnetization of $+1$ unit and the wire contributes the same amount to Δm_{MDR}. A nanowire in the $SD_\downarrow$ state contributes -1 unit to m_0. Its reversal generates an increase of total magnetization of $+2$ units. Then such a wire contributes $+2$ units to Δm_{SDR}. Finally, a nanowire in the $SD_\uparrow$ state just contributes $+1$ unit to m_0. Under these assumptions, the initial fractions of nanowires in the MD, $SD_\downarrow$, and $SD_\uparrow$ magnetic states are simply $x_{MD} = \Delta m_{MDR}$, $x_{SD}^\downarrow = \Delta m_{SDR}/2$, and $x_{SD}^\uparrow = \Delta m_{SDR}/2 + m_0$, respectively. Furthermore, the direction of a given nanowire is determined by a polar angle θ ($0 \leq \theta \leq 90°$) measured, like θ_H, from the upwardly directed normal to the plane of the membrane $\hat{\mathbf{n}}_\uparrow = \hat{\mathbf{z}}$ and an azimuthal angle ψ ($0 \leq \psi < 360°$) measured from the $\hat{\mathbf{x}}$ axis. As a last ingredient of the model, the dispersion in the nanowire directions is assumed to be such that (i) the number of wires the direction of which has an azimuthal angle in the interval $[\psi, \psi + d\psi]$ is independent of ψ (Ref. 26), and (ii) the number of nanowires the direction of which makes an angle with $\hat{\mathbf{n}}_\uparrow$ in the interval $[\theta, \theta + d\theta]$ is given by

$$dN(\theta) = f(\theta)\sin\theta\, d\theta, = \frac{N^*}{\sigma_\theta \sqrt{2\pi}} \exp\left[-\frac{\theta^2}{2\sigma_\theta^2}\right] \sin\theta\, d\theta,$$
(1)

where $\sigma_\theta \ll 90°$ is the standard deviation of the polar angle distribution $f(\theta)$, assumed to be Gaussian, and N^* is a normalization factor such that

$$\int_0^{360°} d\psi \int_0^{90°} f(\theta)\sin\theta\, d\theta = N.$$
(2)

The best simulations of the variations of m_0, Δm_{SDR}, and Δm_{MDR} as a function of θ_H that could possibly be obtained under the given assumptions are shown in Fig. 9. The experimental data are well reproduced for both Ni and Co nanowire arrays. This suggests that the assumptions that we made are appropriate. In particular, the one concerning the dispersion in the wire directions [Eq. (1)] seems justified.

The dispersion in the wire directions as deduced from our analysis is small since $\sigma_\theta = (3.1 \pm 0.1)°$ for Ni and $\sigma_\theta = (3.5 \pm 0.1)°$ for Co. It is so small that the relaxation of the magnetization toward the revolution axis in those nanowires not perfectly aligned along the normal to the plane of the membrane, which occurs as the strength of the external field is reduced from saturation to zero, gives rise to a reduction of magnetic signal of only 0.2%, as further calculated from our

model. This reduction is indeed barely perceptible experimentally, as already mentioned in Sec. III C 2. Moreover, the dispersion in the wire directions is found very similar in the two arrays. This was expected as the two polycarbonate templates supporting these arrays were fabricated in the very same experimental conditions.

To obtain precise information on the angular distribution of the nanopores in such templates is a rather difficult task. To our knowledge, no experimental technique exists which allows to achieve this directly, i.e., for templates with empty pores. Though indirect, magnetic measurements on templates having their pores filled with ferromagnetic materials are one of the only ways, if not the only one, to perform such a characterization. In the past, several experimental methods were developed to determine the distribution of easy axes of magnetization in ferromagnetic fine-particle systems.[27–30] However, implementing any of these methods, generally based on maximum remanence measurements, in the case of the nanowires studied would have been pointless as all of them are strictly restricted to particles, interacting or not, having only two possible (single-domain) states at remanence, and presenting fairly broad distributions of easy axes, two conditions which are not fulfilled in our case. In these conditions, the method presented in this paper deserves to be noticed for its originality and unprecedented sensitivity.

The critical angles (ϵ) of the Ni and Co arrays are both extremely small as they amount to $(2.6 \pm 0.1)°$ and $(1.6 \pm 0.1)°$ respectively. This confirms that the saturating field must indeed be oriented extremely close to the plane normal to a wire for a multidomain state to be realized in this wire after $\mathbf{H}_{sat}$ is removed. This also accounts for the relatively strong difficulty we had in observing such multidomain state by MFM. However, the two angles are significantly different from each other: ϵ is larger in the case of the Ni nanowire array than in the case of the Co nanowire array. As a corollary, the fraction of nanowires which split into domains after the application of $\mathbf{H}_{sat}$ at $\theta_H = 90°$ is much larger in the first case ($x_{MD} = 0.62$ for Ni) than in the second ($x_{MD} = 0.36$ for Co). This might first be related to the much lower parallel-to-wire magnetic anisotropy of the Ni nanowires, as compared to the Co nanowires (see Sec. III A). Indeed, to a much lower magnetic anisotropy corresponds a much smaller torque exerted on the magnetization when oriented at a large angle from the wire axis, which probably facilitates the splitting in domains of opposite longitudinal magnetization component as the saturating field is released. Second, this might also be due in part to the larger number of magnetic defects present in the Ni nanowires, as compared to the Co nanowires (see Secs. II and V), these defects being preferential sites for the formation of domain walls as $\mathbf{H}_{sat}$ is removed.

V. SIMULATION OF THE LONGITUDINAL MAGNETIZATION CURVES

In the analysis of the magnetization measurements that precedes several crucial questions have not been answered or only answered partially. In particular, the double-peak shape of the SDR and MDR components of the $\chi(H)$ curves has

not been accounted for. It is the aim of the present section to answer these questions.

For this purpose, we developed Monte Carlo-*like* numerical simulations. These are based on the following assumptions. The reversal of single-domain nanowires and the re-magnetization of nanowires initially in a multidomain state occur according to the magnetization processes described in Sec. III C. The arrays contain N nanowires ($N = 10^6$ for the computation). With each nanowire one associates two nucleation fields H_n (one per extremity), N_{PS} pinning centers randomly located along the wire, N_{PS} propagation fields H_p (one per pinning center), and, in the case of a multidomain nanowire, an initial number of N_{DW} domain walls. Each of these walls is located on a site chosen at random among the N_{PS} defect sites (which implies $N_{DW} \leq N_{PS}$). The walls are assumed to be infinitely thin so that the amount of magnetization involved in them can be neglected.[31] The nucleation fields H_n and propagation fields H_p are assumed to be distributed according either to a Gaussian statistical law of the form

$$P_{n,p}(H_{n,p}) = \frac{1}{\sigma_{n,p}\sqrt{2\pi}}\exp\left[-\frac{(H_{n,p}-H_{n,p}^0)^2}{2\sigma_{n,p}^2}\right], \quad (3)$$

where $\sigma_{n,p}$ and $H_{n,p}^0$ are respectively the standard deviation and average value of the distribution, or to a log-normal law[32] of the form

$$P_{n,p}(H_{n,p}) = \frac{1}{\beta_{n,p}\sqrt{2\pi}(H_{n,p}-\delta_{n,p})}$$
$$\times \exp\left[\frac{-(\ln(H_{n,p}-\delta_{n,p})-\alpha_{n,p})^2}{2\beta_{n,p}^2}\right], \quad (4)$$

where $\alpha_{n,p}$ and $\delta_{n,p}$ are respectively a scaling parameter and an offset field controlling the position of the distribution, and $\beta_{n,p}$ is a fluctuation parameter controlling its shape (width). The physical origin of the spread in the values of H_n and H_p will be discussed later in this paper (Sec. V D).

In a first attempt to simulate the magnetization curves, N_{PS} and N_{DW} were assumed to vary from wire to wire according to narrow Gaussian probability laws. However, this complication proved almost useless as it appeared that the shape of the $m(H)$ and $\chi(H)$ curves is essentially determined by the average numbers of pinning sites and domain walls. Then, to reduce as much as possible the number of adjustable parameters in the simulations we assigned the same number of defects and walls to all the wires in a given array.

Unfortunately, the guidelines that may be used for choosing the $P_n(H_n)$ and $P_p(H_p)$ probability distributions are very scarce. As a result, the identification of $P_n(H_n)$ and $P_p(H_p)$ is necessarily based on a trial-and-error process. The different steps that were necessary to achieve the identification will now be described in details as this description is essential to establish the conclusions that will be reached eventually.
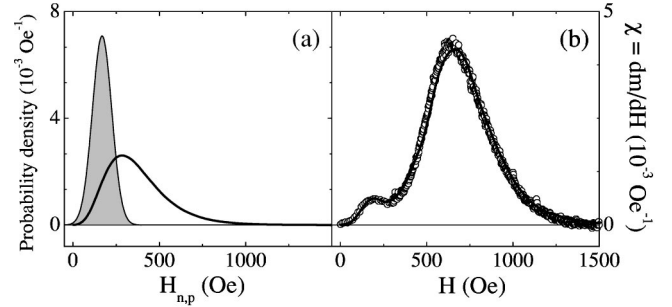

FIG. 10. Result of the first step of the identification procedure in the case of the Ni nanowire array. (a) Distributions of nucleation fields (thin line, shaded curve) and propagation fields (thick line) used to simulate the $\chi(H)$ curve obtained for $\theta_H = 180°$ (SDR component). (b) Experimental (circles) and computed (line) $\chi(H)$ curves.

A. First step

Let us first focus on the $\chi(H)$ curve obtained for $\theta_H = 180°$ (Figs. 7 and 8), i.e., on the SDR component. As one starts from a single-domain nanowire assembly in zero field, no change in magnetization is expected in this case until a first domain wall is nucleated in a nanowire. The smallest field where $\chi(H)$ takes a value significantly different from zero then constitutes an estimate of the smallest nucleation field H_n^{min}, and hence a lower bound for $P_n(H_n)$. The field at which the saturation is reached H_S is the one required for the completion of the reversal of the last nanowire not yet fully magnetized in the field direction. On the other hand, it is known from MFM and transport experiments (see Sec. III C) that, in a vast majority of nanowires, walls nucleated at the extremities undergo pinning during the magnetization reversal. In other words, there generally exists pinning centers (defects) with propagation fields such that $H_p > H_n$. H_S can then be regarded as an estimate of the largest propagation field H_p^{max}, hence an upper bound for $P_p(H_p)$. These few considerations were the starting point of our search for the $P_n(H_n)$ and $P_p(H_p)$ distributions.

Figure 10 shows the result of the first step of the identification procedure, in the case of the Ni nanowire array. The experimental data are well reproduced [Fig. 10(b)]. For this simulation we assumed a number of pinning sites of $N_{PS} = 26$, a Gaussian distribution of nucleation fields ($H_n^0 = 168$ Oe, $\sigma_n = 56$ Oe), and a log-normal distribution of propagation fields ($\alpha_p = 5.83$, $\delta_p = 0$ Oe, $\beta_p = 0.43$) [Fig. 10(a)]. The use of a log-normal $P_p(H_p)$ distribution, as opposed to a Gaussian one, was absolutely necessary in this case to account for the long tail at high fields of the SDR component. It is noteworthy that among the 26 pinning sites introduced here, only two of them (on average) are effective in trapping walls during the magnetization reversal. Notice also that we deliberately used a $P_p(H_p)$ distribution with a non-negligible probability of having defects with small pinning strength (several tens of Oersteds). This choice was made since there is *a priori* no reason for such magnetic defects not to exist in the nanowires. However, simulations as good as the one presented in Fig. 10 could also be obtained with $P_p(H_p)$ distributions such that $P_p(H_p) \simeq 0$ up to
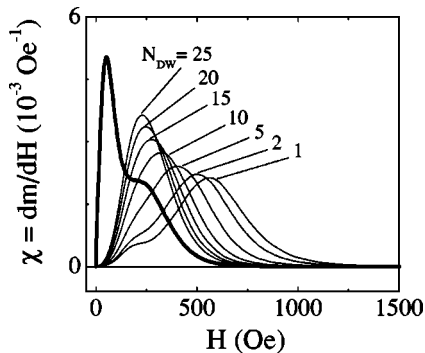
FIG. 11. Experimental MDR component (thick line) and theoretical MDR components (thin lines) computed assuming the nucleation and propagation field distributions of step No. 1 (Fig. 10), for different initial numbers of domain walls N_{DW}.

rather large values of H_p (typically $H_p < 0.6 H_n^0$). This is a trivial consequence of the fact that pinning centers with $H_p < H_n$ are not efficient during the reversal of single-domain nanowires, hence do not affect in any way the SDR curve. The main outcome of step No. 1 is the confirmation that to account for the shape of the SDR component the maximum of the propagation field distribution $P_p(H_p)$ must indeed be located above the maximum of the nucleation field distribution $P_n(H_n)$ and that the width of these distributions must be such that they do not overlap strongly, so that typically $H_p > H_n$. In these conditions only, a vast majority of nanowires reverses its magnetization in several (two or more) well defined consecutive steps reflecting in the non-trivial shape of the SDR curve. Another outcome of step No. 1, of practical relevance, is that for given $P_n(H_n)$ and $P_p(H_p)$ distributions, the height of the low field peak in the SDR component is mostly determined by the number of pinning sites: The larger N_{PS} the smaller this peak.

B. Second step

Of course, for our model to be self-consistent, a given set of statistical parameters should allow to reproduce both the SDR and MDR components of the $\chi(H)$ curves. Therefore, we used the statistical parameters determined in the first step (Sec. V A) to compute the corresponding MDR component. At this point, we restricted our analysis to the MDR curve obtained for $\theta_H = 90°$. Several simulations were made in which the number of domain walls present initially in the nanowires N_{DW} was varied from 1 to 25. It may be seen in Fig. 11 that, with increasing N_{DW}, the remagnetization of the nanowire array occurs in smaller and smaller fields. Moreover the shape of the MDR component changes continuously from the double-peak shape of the SDR component ($N_{DW} = 0$) to a single-peak shape (for $N_{DW} \geq 10$). These two features are related to the fact that, as N_{DW} increases, more and more of the magnetization changes are due to the propagation of walls existing initially, rather than to the motion of walls nucleated at the wire extremities, and among the initially existing walls those which are the most weakly pinned play an increasingly important role. It is obvious though from Fig. 11 that the double-peak structure of the MDR com-

ponent is not reproduced in the simulations. It seems that among the two peaks that the experimental MDR curve exhibits only the one located at high fields may be reproduced under the assumptions made so far (see the curve computed for $N_{DW} = 25$). Interestingly, the same conclusion was reached in the case of the Co nanowire array (an analysis not reported here). Thus it appears clearly, at this stage, that an essential ingredient is missing in our model.

C. Third step

The peak that is absent in the computed MDR component is the one at lower fields (Fig. 11). In the case of the Ni nanowire array, this peak has its maximum at 46 Oe, that is well below the typical nucleation field $H_n^0 = 168$ Oe, and it extends up to approximately 200 Oe. It is related to the propagation of walls which are initially weakly or very weakly pinned ($H_p < H_n$ typically). Its surface area is of the same order of magnitude as that of the high field peak of the MDR component which, according to what precedes, likely corresponds to the propagation of walls departing from sites such that $H_p \gtrsim H_n$ (typically). Hence the initial proportion of weakly pinned walls is certainly large. In these conditions the proportion of defects with small pinning strength must be large too. It is easy to persuade oneself that this high proportion of weak defects is in contradiction with the assumption of a (unimodal) propagation field distribution having a single maximum located above H_n^0, as the one that had to be introduced in the first step to account for the double-peak shape of the SDR component. It occurs that the only way to resolve this inconsistency and reproduce the complex structure of both the SDR and MDR experimental curves is to assume that $P_p(H_p)$ is a bimodal distribution with two well separated maxima, one located above H_n^0, the other one located below H_n^0.

In practice, we built such a $P_p(H_p)$ distribution by simply adding two normalized lines, $P_p^W(H_p)$ and $P_p^S(H_p)$, either Gaussian [Eq. (3)] or log-normal [Eq. (4)], weighted respectively by the fractions of so-called weak pinning sites, x_p^W, and strong pinning sites $x_p^S = 1 - x_p^W$. Such a decomposition in terms of weak and strong pinning sites is somewhat arbitrary since the two lines that compose $P_p(H_p)$ overlap necessarily, as we will see in the sequel. However, it will allow us to extract real numbers from the simulations for the sites of the two kinds, which will be particularly useful when it will come to explaining and justifying physically the existence of two distinct sorts of magnetic defects in the nanowires (see end of this section). Figures 12(a) and 13(a) show the final result of the identification procedure carried out for the Ni and Co nanowire arrays. As announced just before, the $P_p(H_p)$ distributions do not consist of two fully separated lines. However, the overlapping of the lines is sufficiently small so that the low and high field peaks of the MDR component can still, in first approximation, be attributed to the propagation of walls located initially on so-called weak and strong pinning sites, respectively. As a consequence, the relative surface areas of the two peaks constitute rather accurate measures of the fractions of sites of the two kinds present in the nanowires, hence of the weights of the
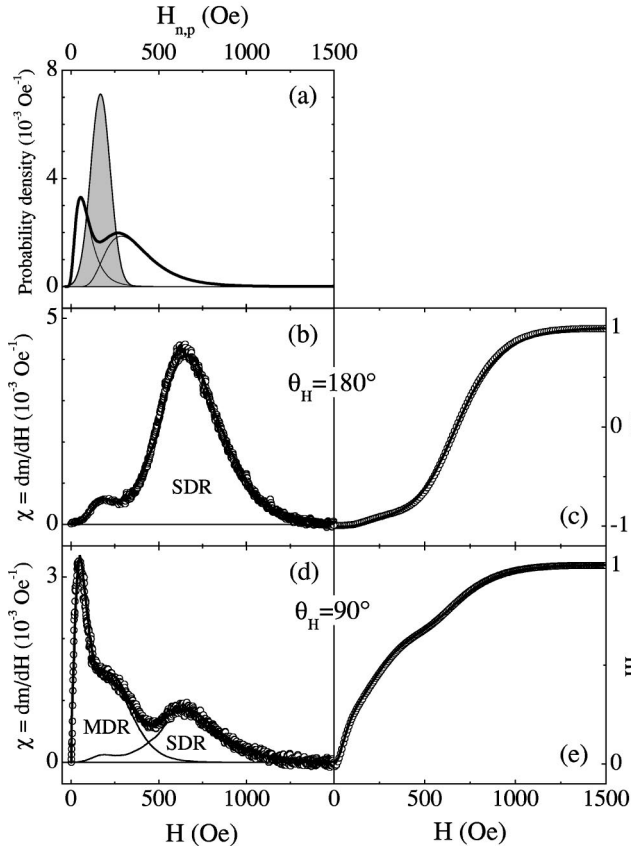
FIG. 12. Final result of the identification procedure in the case of the Ni nanowire array. (a) Distributions of nucleation fields (thin line, shaded curve) and propagation fields (thick line). Experimental (circles) and theoretical (lines) $\chi(H)$ [(b) and (d)] and $m(H)$ [(c) and (e)] curves. The experimental data are those obtained for [(b) and (c)] $\theta_H = 180°$ and [(d) and (e)] $\theta_H = 90°$.

two lines that must be added for building $P_p(H_p)$. This property was naturally used to guide the choice of the parameter x_p^W.

It may be seen in Figs. 12 and 13 that sets of statistical parameters could finally be found, which allow one to reproduce simultaneously all of the experimental data accurately. Figures 12(b), 12(c), 13(b), and 13(c) show the best simulations of the $m(H)$ and $\chi(H)$ curves obtained for $\theta_H = 180°$, that is the most simple case since the data contain only a SDR contribution ($x_{MD} = x_{SD}^\uparrow = 0$, $x_{SD}^\downarrow = 1$). Figures 12(d), 12(e), 13(d), and 13(e) show the best simulations of the experimental data obtained for $\theta_H = 90°$. In this case the magnetization curves contain both a SDR component and a MDR component (see Sec. IV B). For these simulations the fraction of nanowires in the MD state the remagnetization of which gives rise to the MDR component, x_{MD}, and the fraction of nanowires in the SD$_\downarrow$ state the reversal of which manifests itself in the SDR component, $x_{SD}^\downarrow$, were set to the values of Δm_{MDR} and $\Delta m_{SDR}/2$ at $\theta_H = 90°$, as determined in Sec. IV C.

D. Discussion

Table I is a summary of the parameters used for the simulations of Figs. 12 and 13. These call immediately for three
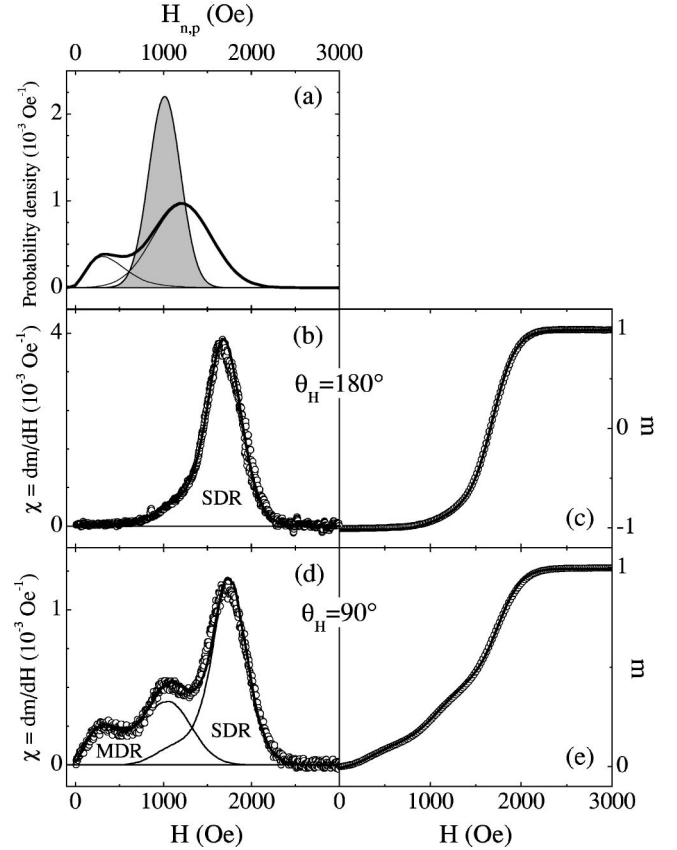

FIG. 13. Final result of the identification procedure in the case of the Co nanowire array. (a) Distributions of nucleation fields (thin line, shaded curve) and propagation fields (thick line). Experimental (circles) and theoretical (lines) $\chi(H)$ [(b) and (d)] and $m(H)$ [(c) and (e)] curves. The experimental data are those obtained for [(b) and (c)] $\theta_H = 180°$ and [(d) and (e)] $\theta_H = 90°$.

comments. First, the number of domain walls that had to be introduced to reproduce the MDR curves ($N_{DW} = 35$ for Ni and $N_{DW} = 29$ for Co) might appear as very large in comparison with the number of walls shown in the MFM image of Fig. 4(d) (five walls in a 10-μm-long wire fragment). Though they are not consistent with the particular MFM image of Fig. 4(d), the values of N_{DW} are not inconsistent with observations by MFM in general. Indeed, up to ten walls were observed by other authors[33] in similar nanowire fragments, 7 μm in length. This corresponds to an average wall density of 10/7 per micrometer which, if applied to the case of our 22-μm-long wires, leads to a number of walls of 31 in good quantitative agreement with the value of N_{DW} used in the simulations ($N_{DW} = 29$ for Co). Furthermore, MFM observations suggest that even higher wall densities might be possible in our nanowires. For example, the adjacent black and white contrasts close to the upper extremity of the wire of Fig. 4(d) stem from two 180° domain walls only 200 nm apart from each other, a distance equivalent to a density of 5 walls per micrometer.

Second, while the fraction of nanowires which split into domains after transverse saturation (x_{MD}) is very different for Ni and Co (also see Sec. IV D), our simulations reveal that the number of walls the multidomain wires contain

TABLE I. Parameters used for the simulations of Figs. 12 and 13 (see the text for details).

	Ni nanowire array	Co nanowire array
Nucleation	Gaussian $P_n(H_n)$ $H_n^0 = 168$ Oe $\sigma_n = 56$ Oe	Gaussian $P_n(H_n)$ $H_n^0 = 1016$ Oe $\sigma_n = 180$ Oe
Weak pinning	Log-normal $P_p^W(H_p)$ $\alpha_p^W = 4.69$ $\beta_p^W = 0.50$ $\delta_p^W = -30$ Oe $x_p^W = 0.40$	Log-normal $P_p^W(H_p)$ $\alpha_p^W = 6.54$ $\beta_p^W = 0.33$ $\delta_p^W = -308$ Oe $x_p^W = 0.19$
Strong pinning	Log-normal $P_p^S(H_p)$ $\alpha_p^S = 5.83$ $\beta_p^S = 0.43$ $\delta_p^S = 0$ $x_p^S = 0.60$	Gaussian $P_p^S(H_p)$ $H_p^{0S} = 1212$ Oe $\sigma_p^S = 332$ Oe $x_p^S = 0.81$
Number of pinning sites	$N_{PS} = 43$ $N_{PS}^W \sim 17$ $N_{PS}^S \sim 26$	$N_{PS} = 32$ $N_{PS}^W \sim 6$ $N_{PS}^S \sim 26$
SDR component	$N_{DW} = 0$	$N_{DW} = 0$
MDR component	$N_{DW} = 35$	$N_{DW} = 29$
$\theta_H = 180°$ experiment $\theta_H = 90°$ experiment	$x_{SD}^\uparrow = 0.00$ $x_{SD}^\downarrow = 1.00$ $x_{MD} = 0.00$ $x_{SD}^\uparrow = 0.19$ $x_{SD}^\downarrow = 0.19$ $x_{MD} = 0.62$	$x_{SD}^\uparrow = 0.00$ $x_{SD}^\downarrow = 1.00$ $x_{MD} = 0.00$ $x_{SD}^\uparrow = 0.32$ $x_{SD}^\downarrow = 0.32$ $x_{MD} = 0.36$

(N_{DW}) is rather similar for the two ferromagnetic metals. This suggests that N_{DW} is mainly determined by the quantity of defects (N_{PS}) present in the nanowires, which only slightly differs between Ni and Co, rather than by the intrinsic magnetic parameters of the materials (e.g., anisotropy, saturation magnetization) which on the contrary are strongly unlike for the two systems.

Third, while the number of strong pinning sites $N_{PS}^S = x_p^S \times N_{PS}$ is the same in the two kinds of wires ($N_{PS}^S \sim 26$), the number of weak pinning sites $N_{PS}^W = x_p^W \times N_{PS}$ is about three times larger in the Ni nanowires ($N_{PS}^W \sim 17$) than in the Co nanowires ($N_{PS}^W \sim 6$). This practical result will be of deciding help in identifying the physical nature of the two classes of defects, which is done next. It is known from the structural characterization evoked in Sec. II that Ni and Co nanowires differ noticeably from one another in the size of the crystal grains they are made of or, in other words, in the number of grain boundaries they contain: Ni nanowires contain more of these defects than Co nanowires. This constitutes a strong indication that the weakest defects may well be grain boundaries, which, as every magnetic inhomogeneities, can act as pinning centers. As far as surface roughness is concerned, Ni and Co nanowires are very similar. Rather important constrictions (Fig. 2) are present along both kinds of nanowires, in similar quantities. Moreover, such constrictions or necks can obviously be extremely efficient in trapping propagating walls, constitute preferential sites for their formation and easily give rise to pinning strength of several hundred or a few thousand Oersteds. It is then reasonable to identify the strongest defects with local reductions of wire diameter. In the light of these results, the variation of the shape of the MDR component with θ_H observed in the case of the Ni nanowire array may be attributed to the fact that as $\mathbf{H}_{sat}$ is removed domain walls form preferentially on sites of a certain kind, for instance on strong defects rather than on weak defects, depending on the precise orientation of $\mathbf{H}_{sat}$ with respect to the wire axis, hence with respect to the membrane normal. This possibility was implicitly ignored in our model.

Our previous experimental observations[13,18] had led us to the conclusion that the vast majority of nanowires reverses its magnetization in several consecutive steps. Nevertheless, there might *a priori* exist a few wires in which all of the defects are such that $H_n > H_p$, so that the magnetization reverses in a simple one-step process, without pinning of the walls nucleated at the extremities. The proportion of wires behaving like this being a question of interest, it has been estimated from our model simulations. In the case of Co, only several tens of wires out of one million have been found to reverse in one go. In the case of Ni, not a single wire has been found to behave like this. These numbers highlight the deciding role of defects in the magnetization processes of electrodeposited nanowires of small diameter.

As may be seen in Fig. 12, the field position and span of the low field peak in the SDR component coincide very well with those of the nucleation field distribution $P_n(H_n)$. The low field peak may thus be definitely attributed to the motion of domain walls which, after being nucleated at a wire extremity, propagate until they are pinned *for the first time*. From the small surface area of this peak, it may be inferred that, on average, the defects where this occurs are located rather close to the extremities where the walls ''enter'' the wires. In contrast, the position of the high field peak in the SDR component does not coincide with that of the high field part of the propagation field distribution $P_n^S(H_n)$, contrary to what one might have naively expected. This phenomenon is again related to the property that pinning centers with $H_p < H_n$ do not trap walls during the magnetization reversal of single-domain nanowires (but they may of course do so during the remagnetization of multidomain wires). Conse-

quently, the peak at high fields corresponds essentially to the propagation of walls departing from sites such that $H_p > H_n$; it thus extends over the field range defined in good approximation by $P_p(H) > P_n(H)$, as verified for both Ni and Co nanowire arrays. In the case of the Ni nanowire array (Fig. 12), the high field peak in the SDR component may still appear to the reader as located at surprisingly large fields with respect to $P_p^S(H_p)$. Its maximum is indeed located in the tail of $P_p^S(H_p)$. This phenomenon is however not unexpected. It is an intrinsic consequence of the fact that $P_p^S(H_p)$ is a log-normal distribution, i.e., a strongly asymmetric distribution with a long tail extending far at large H_p. For such a statistical distribution, which belongs to the class of "broad" distributions (as opposed to "narrow" symmetrical distributions such as Gaussian or normal deviates), it is known that rare statistical events (here large values of H_p) play an unusual dominant role.[34] Translated into terms appropriate in the context of this study, the domination of rare events is the property that the magnetization reversal in the Ni nanowires is mostly determined by very few pinning sites with relatively large propagation fields.

The spread of the values of H_n and H_p has several possible sources. First, it may be due to intrinsic reasons. In the case of the nucleation field these may be fluctuations in the wire diameter or variations in the shape of the wire extremities, such as those evoked in Sec. II. Indeed, it was demonstrated experimentally in the case of elongated nanoscale elements with longitudinal magnetization that smaller lateral dimensions and/or sharper ends give rise to enhanced switching fields.[2,35,36] As for the propagation field, intrinsic reasons for fluctuations are trivial: These are variations in the nature and/or the size of the defects.

The average distance between the pores (1 μm) being only a fraction of the wire length ($L = 22$ μm), significant dipolar interactions between the nanowires probably exist in the studied arrays. These may affect the nucleation and propagation fields in several ways. To demonstrate this point in a simple manner, let us consider the following two extreme situations. In the first one, all the wires are single-domain and their magnetization vectors are aligned antiparallel to the external field. This is what the magnetic configuration of the array is just before the reversal starts. In the second, an external field has been applied, whose magnitude was large enough so that a large number of wires has reversed its magnetization. This corresponds to the end of the reversal process, just before the magnetization of the array reaches saturation. In the first situation, the dipolar field generated by the neighboring wires on any particular wire adds to the external field.[17] As compared to an equivalent but isolated wire, the wire in question is thus exposed to a larger effective field; nucleation and propagation are therefore promoted by the dipolar interactions and occur in smaller applied field. In the second situation, those wires which are still magnetized antiparallel to the applied field are mostly surrounded by neighbors which have reversed their magnetization. These antiparallel wires are then confronted to a dipolar field opposite to the external field,[17] and hence to a reduced effective field. Nucleation and propagation in these wires occur therefore at larger applied field strength, as compared

to noninteracting wires. This clearly shows that magnetostatic interactions between wires can be a source of broadening of the characteristic field distributions. The fact that the same $P_n^S(H_n)$ and $P_p^S(H_p)$ distributions could be used to simulate the $\chi(H)$ and $m(H)$ curves corresponding to the reversal of single-domain wires *and* to the remagnetization of multidomain wires suggests however that dipolar interactions are not the dominant source of spread in the values of H_n and H_p. If this were the case, the $P_n^S(H_n)$ and $P_p^S(H_p)$ distributions would depend more strongly on the details of the magnetic structures inside the wires, hence on the type of magnetization process.

Finally, the distributions of H_n and H_p values are certainly also due in part to an extrinsic reason that is the imperfect parallel alignment of the nanowires. It is unlikely that a misalignment of a few degrees of the external field with respect to the wire axis (see Sec. IV D) may modify deeply the mechanisms of reversal and remagnetization. However it is reasonable to assume that such a misalignment may slightly affect both H_n and H_p. Although the impact of this extrinsic source of disorder is hard to quantify, it is believed that the spread of H_n and H_p reflects mainly differences in the intrinsic properties of the nanowires.

VI. CONCLUSION

We have shown that the analysis and modeling of usual magnetization measurements can yield valuable statistical information on the magnetic properties of arrays of several million ferromagnetic nanowires. The information obtained concerns the statistical distribution of the wire orientation, nucleation field, and strength of the pinning centers. The analysis required the knowledge of the underlying magnetization processes and domain structures, gained from previous experimental investigations.

The data that were analyzed are the first longitudinal magnetization curves measured after the application of a saturating magnetic field at different angle with respect to the average direction of the nanowires. These curves may contain two clearly identifiable components corresponding to the reversal of single-domain nanowires and to the remagnetization to saturation of multidomain nanowires, respectively. The distribution of wire orientation was deduced from the angular variation of the amplitude of these two components. From the modeling of the shape of the two components, it was shown that two distinct kinds of defects with very different pinning strengths are certainly present in the nanowires. These were tentatively identified as grain boundaries and constrictions.

*Electronic address: Yves.Henry@ipcms.u-strasbg.fr

[1] M. Hehn, K. Ounadjela, J.-P. Bucher, F. Rousseaux, D. Decanini, B. Bartenlian, and C. Chappert, Science **272**, 1782 (1996).

[2] S. Y. Chou, Proc. IEEE **85**, 652 (1997), and references therein.

[3] D. J. Sellmyer, M. Zheng, and R. Skomski, J. Phys. Condens. Matter **13**, R433 (2001), and references therein.

[4] C. R. Martin, Adv. Mater. **3**, 457 (1991).

[5] T. M. Whitney, J. S. Jiang, P. C. Searson, and C. L. Chien, Science **261**, 1316 (1993).

[6] I. Chlebny, B. Doudin, J.-P. Ansermet, Nanostruct. Mater. **2**, 637 (1993).

[7] A. Fert, L. Piraux, J. Magn. Magn. Mater. **200**, 338 (1999), and references therein.

[8] Y. Henry, K. Ounadjela, L. Piraux, S. Dubois, J.-M. George, and J.-L. Duvall, Eur. Phys. J. B **20**, 35 (2001).

[9] W. Wernsdorfer, B. Doudin, D. Mailly, K. Hasselbach, A. Benoit, J. Meier, J.-Ph. Ansermet, and B. Barbara, Phys. Rev. Lett. **77**, 1873 (1996).

[10] W. Wernsdorfer, K. Hasselbach, A. Benoit, B. Barbara, B. Doudin, J. Meier, J.-Ph. Ansermet, and D. Mailly, Phys. Rev. B **55**, 11 552 (1997).

[11] R. O'Barr and S. Schultz, J. Appl. Phys. **81**, 5458 (1997).

[12] J.-E. Wegrowe, D. Kelly, A. Franck, S. E. Gilbert, and J.-Ph. Ansermet, Phys. Rev. Lett. **82**, 3681 (1999).

[13] U. Ebels, A. Radulescu, Y. Henry, L. Piraux, and K. Ounadjela, Phys. Rev. Lett. **84**, 983 (2000).

[14] A. Aharoni, *Introduction to the Theory of Ferromagnetism* (Oxford University Press, Oxford, 1996).

[15] R. Skomski and J. M. D. Coey, *Permanent Magnetism* (Institute of Physics, Bristol, 1999).

[16] R. Skomski, H. Zeng, M. Zheng, and D. J. Sellmyer, Phys. Rev. B **62**, 3900 (2000).

[17] R. Hertel, J. Appl. Phys. **90**, 5752 (2001).

[18] A. Radulescu, U. Ebels, Y. Henry, K. Ounadjela, J.-L. Duvall, and L. Piraux, IEEE Trans. Magn. **36**, 3062 (2000).

[19] E. Ferain and R. Legras, Nucl. Instrum. Methods Phys. Res. B **82**, 539 (1993); **84**, 331 (1994); **131**, 97 (1997).

[20] S. Pignard, G. Goglio, A. Radulescu, L. Piraux, S. Dubois, A. Declémy, and J.-L. Duvall, J. Appl. Phys. **87**, 824 (2000); S. Dubois, J. Colin, J. L. Duvall, and L. Piraux, Phys. Rev. B **61**, 14 315 (2000).

[21] See, for example, M. Emura, D. R. Cornejo, and F. P. Missell, J. Appl. Phys. **87**, 1387 (2000).

[22] The statement that the nanowire arrays studied consist of two equally large populations of single-domain entities after demagnetization by means of an alternating field applied parallel to the average wire direction is deduced from the observation that the first magnetization curve measured after such a demagnetization

procedure $M_{ini}(H)$ and the major hysteresis loop $M(H)$ approximately obey the relationship $M_{ini}(H)=(M(H)+M_S)/2$ (see Fig. 5). The field independent contribution to $M_{ini}(H)$, $M_S/2$, is due to this half of the nanowires the magnetization of which is already aligned parallel to the external field **H** after the demagnetization procedure, and the field dependent contribution, $M(H)/2$, to the reversal of the second half of the nanowires the magnetization of which is initially antiparallel to **H**. The fact that the nanowires are generally in a single-domain state after a longitudinal *ac* demagnetization was also observed by MFM (see Ref. 8).

[23] See, for example, R.G. Simmons, IEEE Trans. Magn. **26**, 93 (1990).

[24] The two peaks exhibit very similar variations of their amplitudes with θ_H, which demonstrates their common origin.

[25] In reality, this assumption is certainly not verified exactly for each nanowire in a multidomain state. However, given the large number of nanowires in an array, one may assume that this is true on average.

[26] The arrays of nanowires are assumed to have a rotational symmetry, with the normal to the plane of the membrane as symmetry axis. This assumption is justified by the fact that these arrays do not exhibit any kind of anisotropy of their magnetic properties in the plane of the membrane and is consistent with the process of fabrication of the templates (tracks obtained by irradiation under normal ion beam incidence; see Sec. II).

[27] S. Shtrikman and D. Treves, J. Appl. Phys. **31**, 58S (1960).

[28] F. Cebollada, M. F. Rossignol, D. Givord, V. Villas-Boas, and J. M. González, Phys. Rev. B **52**, 13 511 (1995).

[29] J. W. Harrell, Y. Yu, Y. Ye, J. P. Parakka, D. E. Nikles, and H. G. Zolla, J. Appl. Phys. **81**, 3800 (1997).

[30] R. Iglesias, H. Rubio, and S. Suárez, Appl. Phys. Lett. **73**, 2503 (1998).

[31] This approximation is justified by the experimental observation that the transverse remanent magnetization (Fig. 3) which is a measure of the amount of magnetization involved in the walls is small (respectively 3% and 8% of the saturation magnetization for the Co and Ni nanowire arrays).

[32] Log-normal distributions [Eq. (4)] were only introduced when the use of Gaussian ones [Eq. (3)] could not allow one to reproduce the experimental data satisfactorily.

[33] L. Prejbeanu and U. Ebels (unpublished).

[34] V. Da Costa, Y. Henry, F. Bardou, M. Romeo, and K. Ounadjela, Eur. Phys. J. B **13**, 297 (2000), and references therein.

[35] S. Y. Chou, P. R. Krauss, and L. Kong, J. Appl. Phys. **79**, 6101 (1996).

[36] K. J. Kirk, J. N. Chapman, and C. D. W. Wilkinson, Appl. Phys. Lett. **71**, 539 (1997); J. Appl. Phys. **85**, 5237 (1999).